Initial-vortex-entry-related magnetic hysteresis in thin-film SQUID magnetometers

J. Z. Sun, W. J. Gallagher, and R. H. Koch
IBM Thomas J. Watson Research Center, P.O. Box 218, Yorktown Heights, New York 10598
(Received 6 January 1994; revised manuscript received 9 June 1994)

We report measurements and modeling of magnetic hysteresis in SQUID magnetometers cycled in fields of 0.1 to 10 G peak to peak. We show that the observed hysteresis is caused by the penetration of magnetic vortices around the edges of the superconducting thin-film structures forming the SQUID. A threshold field for the onset of hysteresis is predicted and subsequently observed experimentally. The threshold corresponds to the situation when the Lorentz force driving a vortex into the SQUID washer first exceeds the sum of the surface barrier and pinning forces. The threshold field depends on the pinning strength of the superconducting material forming the edges of the device, and is thus distinguished from the lower critical field, H_{c1}, for flux entry in type-II superconductors. It is, to our knowledge, the first time a threshold field for flux entry is observed to relate to the local pinning strength of a structure. Comparison of our earlier experimental data with model calculations revealed the existence of a degradation in critical current density at edges of our devices. Subsequent optimization of our high-T_c device fabrication process lead to significant improvement in hysteresis characteristics. The threshold field in the improved devices is clearly observable, near which at 77 K a thousandfold reduction in hysteresis is obtained. We believe the mechanism of magnetic flux entry studied in this work is also relevant to the understanding of the hysteresis loss in high-T_c superconductors at microwave frequencies. Such hysteresis, resulting in a strongly power-dependent loss, is a major factor limiting the high-power applications of thin-film high-T_c microwave devices.

INTRODUCTION

One obstacle to pervasive use of SQUID gradiometers in ambient magnetic environments is undesired sensitivity to time-varying background fields. At a value of around 0.5 G, such fields are often high enough to cause flux-trapping-related magnetic hysteresis in the thin films of such devices. It is thus important to understand the origin of this hysteresis. It is known that different parts of a SQUID, such as its washerlike pick-up loop, its input coil, and other ancilary structures, all contribute to the overall hysteresis response of the device.[1-6] Although in most applications the SQUID itself stays in a flux-locked loop, some of these superconducting structures may still be subject to a significant amount of local magnetic field. This is especially the case when the SQUID input consists of coils configured to measure the gradient of applied magnetic field.

In this work, the phenomenon of magnetic hysteresis in the basic sensing element of a thin-film SQUID magnetometer is studied. The observed hysteresis is used to understand the physics of magnetic vortex penetration from the edges of superconducting thin-film structures. A model for flux entry around the edges of thin-film structures has been developed and verified. The model provides a guideline for the reduction of magnetic hysteresis in thin-film device structures. With this understanding, we improved our design and our fabrication process and lowered the magnetic hysteresis in our high-T_c thin-film SQUID's to levels acceptable for operation in ambient fields.

For SQUID magnetometers, magnetic hysteresis refers to the shift of the voltage-flux $V(\Phi)$ transfer function along the Φ axis upon cycling of the applied magnetic field. The hysteresis error can be represented by a net change in the amount of flux coupled into the SQUID loop $\delta\Phi$. Alternately, the effective magnetometer coupling area A_{eff} can be used to define an effective hysteresis

$$\delta H = \delta\Phi / A_{\text{eff}} . \tag{1}$$

Magnetic hysteresis in a SQUID results from displacement or nucleation of magnetic vortices in the superconducting structure of the device. Experimentally, two types of hysteresis have been found. One type of hysteresis involves a time-dependent (exponentially decaying) behavior; the other type is time independent. For Nb–thin-film–based SQUID gradiometer systems tested under magnetic fields well below 1 G, Koch *et al.*[1] found a time-dependent magnetic hysteresis that was linearly dependent on the amplitude of the applied cycling magnetic field. A hysteresis factor h, defined as $\delta H / H_{p\text{-}p}$, where $H_{p\text{-}p}$ represents the peak-to-peak value of the cycling field applied to the sample, was used to quantify the hysteresis characteristic of these Nb-based thin-film SQUID's. This time-dependent hysteresis is believed to be related to the viscous motion of magnetic vortices trapped inside the input-washer structure of the SQUID gradiometer. More recent studies by us[7] indicate that the time-dependent hysteresis is caused by a relaxation type of response of the SQUID, with the characteristic relaxation time depending strongly on the SQUID's operating temperature. The relaxation-time constant is typically in the range of less than a few hundred milliseconds for Nb-based SQUID's at 4.2 K, and is about an order of magnitude smaller for high-T_c SQUID's operating at 77 K. More studies are needed to completely understand

0163-1829/94/50(18)/13664(10)/$06.00

the mechanism of this relaxation. In this paper we will not get into more details of the time-dependent hysteresis of SQUID's, but rather we will focus on time-independent hysteresis.

A significant amount of nonlinear hysteresis was first observed in our early measurements on high-T_c thin-film SQUID's.[8] The granular nature of the early thin films was suspected to be the cause. More recently, we made a comparison study of the hysteresis characteristics of both high-T_c $YBa_2Cu_3O_{7-\delta}$ (YBCO) thin-film SQUID magnetometers and Nb–thin-film SQUID's.[4] To isolate the cause of hysteresis, simple washer-shaped SQUID magnetometers were used as test devices. Measurements were carried out in cycling fields of up to a few Gauss. Both time-dependent hysteresis and time-independent hysteresis were observed in high- and low-T_c SQUID's, and the time-independent hysteresis was studied in some detail. This hysteresis appeared to increase quadratically with the amplitude of the cycling field in this field range. We found a similar temperature dependence between the characteristic hysteresis field and that of the critical current density of the film, which suggested a possible link between hysteresis and vortex pinning. Flux entry around the edges of the washer was suggested as a plausible cause of the onset of such hysteresis. We later developed a quantitative model, which took into account three major factors affecting the penetration of magnetic vortices from the edge of a thin-film superconducting washer structure: the Lorentz driving force, the surface barrier to flux entry, and the defect pinning force.[5] The balance of these three forces was shown in the model to set a threshold field, below which no flux penetration would occur. The magnitude of the threshold field was directly related to the critical current density of the thin-film material at the edge. If this mechanism were controlling the entry of magnetic vortices, then the quality of material at the edge of the washer structure, namely its critical current density and its T_c, would be important factors in determining the hysteresis performance of the device. The experimental data available in that work, however, only hinted at the possible existence of a threshold field for the onset of the nonlinear hysteresis.

In this work, we elaborate on our earlier model[5] for the nonlinear hysteresis and present new measurements on improved devices. The predicted threshold field described in our previous paper[5] is clearly observed, as was briefly described in a preliminary report.[6] The time-independent hysteresis is shown to be directly related to the edge quality of the film around the washer. By improving the quality of film edges in devices after lithographic processing, we demonstrate a decrease in hysteresis by over three orders of magnitude in fields of 2–4 G at 77 K.

There is a vast literature concerned with the magnetic properties of superconductors, and, in particular, flux motion and pinning in the high-T_c materials. (For example, some recent well-referenced studies of superconducting films in perpendicular fields can be found in Refs. 9–11.) Much of this work is at high fields where large numbers of vortices are involved, and a correlation between the transport critical current and the spatial profile of vortex distribution can be established (see, for example, Zeldov *et al.*[10]). Studies presented in this paper, on the other hand, concern effects of initial penetration of individual vortices around edges of device structures, which is sensitively measured with a SQUID.

It is known that individual vortex effects are important, for example, for the determination of the lower critical field H_{c1}. There have been a number of recent studies, primarily on high-T_c crystals, relating to the field at which flux first penetrates as determined by H_{c1} and, in particular, by the surface barrier retarding the initial entry of flux into a superconductor.[12–15]

In spite of these studies, it remains unresolved exactly what determines the initial flux entry in an actual device geometry under cycling applied fields. It is not clear whether or not such penetration is related to the bulk H_{c1} of the material, especially when strong pinning is present. The presence of pinning makes it difficult to use simple H_{c1}-type arguments based on thermodynamics. There continue to be alternative suggestions offered to explain what determines the initial flux entry. For example, Burlachkov *et al.*[16] suggested that local defective regions effectively admit flux at fields near H_{c1}, while Brandt and Indenbom[9] recently suggested that properly accounting for bulk pinning effects can account for the apparent increase in the flux entry field with no need to invoke the surface potential barrier.

Our study presents the first case in which the entry of a single vortex into a thin-film edge structure is directly related to the pinning strength of the material right at the edge, thus revealing the importance of the control of edge materials quality. Furthermore, we present direct experimental verification of this concept by quantitative measurements of the onset threshold field for hysteresis in our devices. These experiments established a clear correlation of the threshold field to sample temperature (and thus to the critical current density, or the pinning strength, of the material) and provides strong support to our understanding of the flux entry mechanism.

MODEL FOR NONLINEAR HYSTERESIS

Magnetic hysteresis in SQUID's comes from the displacement of vortices. Vortices may be trapped in any superconducting part of a SQUID structure during cooling. They can also be formed when applied fields are strong enough to cause the nucleation of new vortices. A major contribution to hysteresis comes from the nucleation and subsequent displacement of vortices around edges of the washer structure. This is because the superconducting shielding current induced by applied fields is concentrated around edges of the washer. This causes vortices around the edge to be the first ones to experience a strong Lorentz force, and thus be depinned and displaced.

We have experimentally evaluated the hysteresis behavior of SQUID structures with different washer shapes—squares and octagons, for example. For washers of similar effective pickup areas A_{eff}, we found that, to within the average sample-to-sample scattering, the hysteresis behavior is insensitive to the shape of the washer

structure. For simplicity of argument, we model the thin-film washer structure in our SQUID's as a circular-shaped ring, with a narrow, low inductance slit connecting the inside and outside. We assume an inner hole of radius R_1, and an outer radius R_2, with $R_1 \ll R_2$. When a field H_a is applied perpendicular to the plane of the ring structure, the sheet current density near the outer rim at a radial position r ($R_2 \geq r \gg R_1$) is estimated to be[17]

$$K_a(r)=\frac{cH_a}{\pi^2}\frac{R_2}{\sqrt{R_2^2-r^2}} . \quad (2)$$

A similar current peak is formed near the inner rim.

In principle, vortex penetration can occur both at the inner rim and at the outer rim. Penetration of a vortex at the outer rim will give a hysteresis of leading phase—which means the $V(\Phi)$ characteristic for the down sweep of the cycling field is displaced from that of the up-sweep curve in the direction of increasing field. Penetration at the inner rim, however, will result in a hysteresis in the opposite direction. We have confirmed this directly by experiments using Nb-based SQUID's. In one such experiment small spots (about 20 μm in diameter) at the outer and inner rim of two test SQUID's were intentionally damaged using laser ablation. The damage resulted in increased magnetic hysteresis. The sign of the hysteresis was consistent with the foregoing discussion. For high-T_c SQUID magnetometers, however, the measured hysteresis almost always had a leading phase, which indicates that vortex penetration occurs most often at the outer rim. We will discuss the reason for such behavior in a later part of the paper. In what follows we will focus our attention on the vortex dynamics around the outer rim. The physics for treating the penetration at the inner edge is essentially the same.

Vortices located near the edge of the SQUID washer experience the strongest Lorentz force due to the peaked current density K_a near the film edge. When the current flow is such that the force exceeds the pinning force on the vortex, it will be driven in by the Lorentz force until that force becomes balanced by the pinning force. Assuming that the film is thin compared to the superconducting penetration depth, the vortices can be well described by a two-dimensional (2D) current distribution similar to that calculated by Clem.[18] When the washer is first cooled in zero field into the superconducting state and then a magnetic field H_a is applied normal to the thin-film plane, the total electromagnetic driving force K_e exerted on a vortex at a position r satisfying $\xi=(R_2-r)/R_2 \ll 1$, can be written as

$$K_e(\xi)=\frac{k_1}{\xi^2}-\frac{k_2 H_a}{\sqrt{\xi}} , \quad (3)$$

in which $k_1=\Phi_0 c/16\pi^2 R_2^2$, $k_2=c/\sqrt{2}\pi^2$, and Φ_0 is the flux quantum. The first term in (3) is the surface barrier to flux entry describing the attraction due to image vortex outside the edge using the vortex interaction summarized in Ref. 18; the second term is the Lorentz force from the shielding current K_a. The forces in Eq. (3) are expressed in terms of equivalent sheet current densities.

Figure 1(a) shows an example comparing the driving force K_e of Eq. (3) for different H_a to the pinning force appropriate for an assumed bulk current density of 10^6 A/cm^2. The shaded area indicated the region where the force on the vortex would be less than the maximum defect-related pinning force, i.e., the local sheet critical current density. A vortex experiencing a driving force above the shaded area will be expelled from the washer, and a vortex experiencing a force below the shaded area will be pushed further into the washer until it reaches a balance point like that labeled A. A vortex experiencing an electromagnetic force K_e less than the maximum pin-

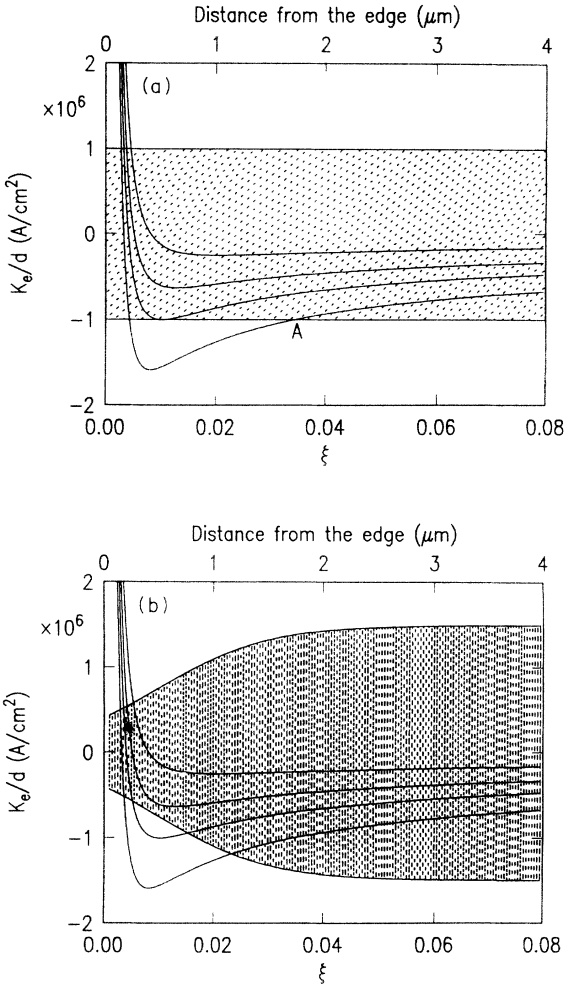

FIG. 1. (a) An illustration of the force balance for a vortex near the edge of a thin-film structure. ξ is the distance of the vortex from the edge, measured in units of R_2. Actual displacement distances are labeled on top of the graph for a representative washer size of $R_2=50$ μm. Forces are expressed in terms of effective current density, where a film thickness of 150nm is assumed. The applied fields H_a for the four curves are, from the top down, 1 G, 2 G, 3.83 G, and 4 G, respectively. The third curve, with $H_a=3.83$ G, corresponds to an applied field just equal to the threshold field value, as calculated by (4). (b) A sketch similar to (a) with critical current density of the film varying with position, illustrating the case of edge-critical current degradation.

ning force, i.e., one described by the curve segments within the shaded region, on the other hand, will remain at its pinning site.

The force balance described by Eq. (3) points toward the existence of a threshold for the applied field H_a, below which the electromagnetic force is insufficient to depin the vortex. The threshold field corresponds to the curve in Fig. 1 that just touches the bottom of the shaded region. Below the field amplitude no vortex displacement or entrance can occur. An expression for the threshold field can be obtained by equating the minimum of Eq. (3) to the bulk pinning force. This yields a threshold field H_{Ta} of

$$H_{\mathrm{Ta}}=\left[\left[\frac{2\pi}{3}\right]^3\frac{\Phi_0}{R_2^2}H^{*3}\right]^{1/4}, \tag{4}$$

where H^* is a characteristic field defined as $H^*=2\pi J_c d/c$. (In practical units $H^*=6.28\times10^{-9}J_c d$, where H^* is in Gauss, J_c in A/cm^2, and d in angstroms.) At this threshold, the nucleated vortex will be at the position

$$\xi_{\mathrm{Ta}}=\left[\frac{3}{8\pi}\frac{\Phi_0}{H^*R_2^2}\right]^{1/2} \tag{5}$$

For H_a above the threshold, any vortex nucleated at the edge will be swept to a point further in than ξ_{Ta}, like point A in Fig. 1, where the electromagnetic force is balanced by the pinning force. Position A, where the vortex is swept to, is plotted in Fig. 2(a) as a function of the applied field for various assumed current densities. The curves begin at the threshold point ξ_{Ta} for each current density and are truncated at the upper end, where the approximations that led to Eq. (2), i.e., ignoring the inner boundary, are no longer valid. In the high H_a limit, the image force can be neglected and the vortex position assumes an asymptotic form of $\xi\simeq(2/\pi^2)(H_a/H^*)^2$. This is likewise valid until ξ becomes so large that the effects of the inner boundary start to become important.

When H_a is reduced to zero and there is no Lorentz force from the shielding currents pulling the vortex into the washer, the vortex will remain trapped at A. Upon the application of $-H_a$, however, this vortex will have a net force far exceeding the pinning force and will be swept out of the washer. A vortex of opposite sign will then be placed at point A. The net hysteresis effect is therefore twice the flux a single vortex couples into the SQUID loop.

The amount of flux a vortex line positioned at ξ couples into the SQUID loop in the two-dimensional (2D) vortex limit can also be estimated. For geometries where $R_2-R_1\ll R_2$, the answer is given in Ref. 1. For our experimental geometry, where $R_2\gg R_1$, the approximation in Ref. 1 is no longer valid, and a different estimate has to be made. This can be done rather easily in the thin film limit, where the film thickness is small compared to the superconducting penetration depth. In this case, which is most relevant for us, one can make an electrostatic analogy[5] based on Clem's observation that [18] the far-field distribution of the flux line of a 2D vortex resembles that of a monopole. The result[5] is that the flux coupled into the SQUID loop, for a vortex sitting at radius r with $R_1<r<R_2$, is

$$\frac{\Phi(r)}{\Phi_0}=\frac{(R_2-r)R_1}{(R_2-R_1)r}\ . \tag{6}$$

Letting r be the position of the balance point A, we can solve numerically for the net flux coupled into the SQUID as a function of sweep field $H_{p\text{-}p}=2H_a$ at fixed current density. This is plotted in Fig. 2(b). For a vortex near the outer rim of the washer Eq. (5) becomes $\Phi(\xi)/\Phi_0\simeq(R_1/R_2)\xi$. Thus the large-field asymptotic form of ξ, when combined with Eq. (5), gives the hysteresis from a single vortex penetrating from the outer rim of the washer as

$$\delta H\simeq\frac{H_0}{\pi^2}\left[\frac{R_1}{R_2}\right]\left[\frac{H_{p\text{-}p}}{H^*}\right]^2 \tag{7}$$

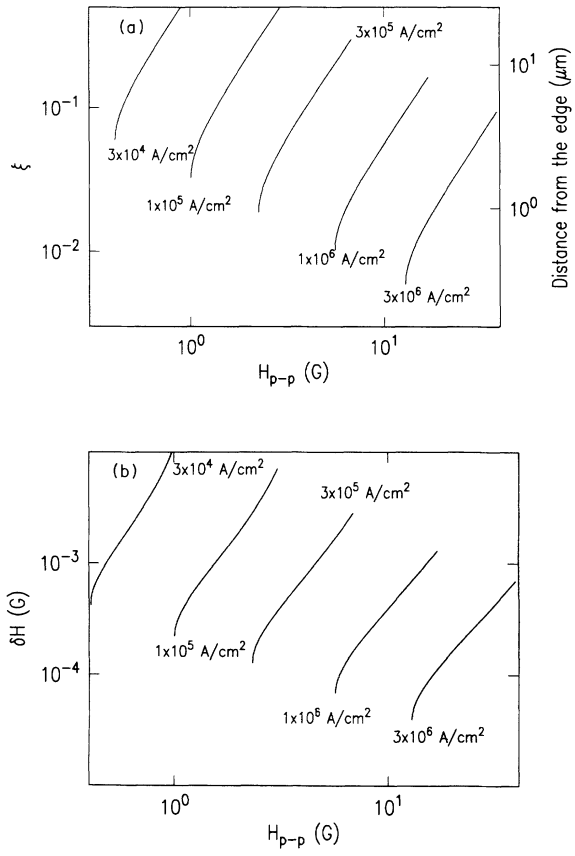

FIG. 2. (a) Amount of displacement for a vortex in a cycling field of peak-to-peak amplitude $H_{p\text{-}p}$ for films with different critical current density. (b) Magnitude of hysteresis such vortex displacement results in a SQUID washer structure. An outer radius of 50 μm and a film thickness of 150 nm was assumed in these calculations. The lowest point on each of these curves is the point on the threshold point where a vortex can first be nucleated over the surface barrier. The upper part of the curves is truncated because for very large vortex displacements, the approximation $r\gg R_1$ is no longer satisfied, and Eq. (3) no longer describes properly the force exerted on the vortex.

for large $H_{p\text{-}p}$, as long as $\delta H/H_0 \ll 1$, where $H_0 = \Phi_0/A_{eff}$ is the periodicity of the SQUID in magnetic field. This asymptotic behavior was seen in our earlier work, but not the threshold effect.

Our notion of a threshold field for hysteresis is similar to that of a critical flux entry field[19] introduced long ago based on the Bean and Livingston surface barrier to flux entry.[20] That flux entry field, however, was the field at which the potential barrier to flux entry disappeared. Considerations for that field did not involve pinning. Our threshold field is by contrast entirely determined by the pinning strength. The conventional flux entry field is an often-used parameter to describe the delayed flux entry or exit from a superconductor and is sometimes referred to as describing the surface pinning.[21] Our Eq. (5) appears to us to be the first such explicit relationship, however. Moreover, our description in Fig. 2(b) of the field dependence of the flux entry above the threshold H_{Ta} is also new. It is also worth noting that the abruptness of the hysteresis increase we predict above the threshold is in marked contrast to the gradual increase in a recent calculation that neglected the surface barrier.[9]

Similar calculations can be made to estimate the onset of nonlinear hysteresis in other thin-film structures, such as thin-film strips or closed loops. Estimates for two such structures are given in the Appendix.

So far we have discussed the process of a single vortex entering the edge of a superconducting thin film washer. We assumed that the local critical current density of the superconducting film is uniform. This, however, may not be true in real devices. Due to lithography-related damage or material's imperfection, material near edges of the structure is likely to suffer a degradation in its superconducting properties, such as T_c and J_c. Such degradation is particularly severe for high-T_c thin films.[5] This may make the quantitative treatment of flux entry difficult. One such possible situation is demonstrated in Fig. 1(b), where the critical current density, or the pinning strength, of the film is allowed to vary as a function of the distance from the edge. It is clear from comparison of Fig. 1(b) with Fig. 1(a) that, while the qualitative features of the flux-entry process remain unchanged and we still may observe a threshold field somewhat representative of the critical current density of the material near the edge, the quantitative results of Eq. (4) and those in Fig. 2 are no longer adequate. As a result of depressed critical current near the edge, one might expect to see an onset of hysteresis below the nominal threshold value as estimated by Eq. (4). At the same time, the onset curvature and magnitude of hysteresis field δH may show significant deviation from that presented in Fig. 2. Thus caution should be exercised in comparing the quantitative details of this model to measurements.

So far we have considered only flux-trapping effects in the outer rim of the washer structure that forms a SQUID. This should be the predominant area of concern. However, other parts of a SQUID may also trap flux, such as the coil. Moreover, the physics of flux entry into thin-film structures discussed in this paper may also apply to performance issues of other thin-film superconducting devices, such as the power dependence of microwave resonators. In the Appendix, we give some useful expressions describing the flux-entry threshold for geometries other than a washer.

EXPERIMENTAL PROCEDURES

Systematic experimental investigations were carried out to understand the nonlinear hysteresis in thin-film dc SQUID's and to make comparisons with the predictions of the model developed in the preceding section. In this section we describe sample preparation and the procedures used for measurements. The results of the measurements, given in the next section, give a clear indication of a threshold behavior for the onset of nonlinear hysteresis, confirming the prediction of our model. A direct correlation between edge-film quality and the hysteresis performance of devices is also observed.

Square washer dc SQUID's were used in this experiment. The inner hole measures 40 μm on each side. Washer outer dimensions of 100 and 240 μm were both investigated. Two types of weak-link junctions were used for these SQUID's: junctions formed across a bicrystal substrate defined grain boundary and junctions formed over a step edge in a substrate. The hysteresis behavior observed did not depend on the type of junctions used.

The fabrication of step edges on $SrTiO_3$ substrates was done by ion milling using a patterned diamondlike-carbon film as a stencil. Step heights typically ranged from 140 to 260 nm. The wall angle of the step was around 65°. A post processing anneal at 800 °C, in 1 atm of oxygen for 2 h was used to help heal the ion milling damage at the steps.

All devices tested to date used a single layer thin film of YBCO. YBCO films, usually having thicknesses between 100 and 250 nm, were deposited *in situ* by pulsed laser deposition. The films were oriented with the *c* axis perpendicular to the surface. Typical transition temperatures T_c ranged between 90 and 92 K, with a critical current density of around 5×10^6 A/cm^2 at 77 K. Patterning of the SQUID structure was done with photolithography and Ar-ion milling. Care was taken in the entire lithographic process not to overheat the YBCO sample, and during the course of these studies several process improvements were undertaken in order to protect YBCO film from process-related degradation. These included (1) coating of the YBCO film with a blank layer of silver 50-nm-thick *in situ* before lithographic processing; (2) using low-energy, low-duty-cycle ion milling (500 V, 0.3 mA/cm^2, and 5-min-on–5-min-off intermittent milling) to minimize the degradation of YBCO caused by excessive heating in an oxygen-poor environment; and (3) reoxygenation of the final device chip in an oxygen plasma as the last step of processing. Details of the fabrication process are described elsewhere.[22]

Two SQUID readout schemes were used during the course of this study. Initially, the SQUID signals were read out directly (dc) with a commercial room-temperature preamplifier. More recently, an ac-modulated readout circuit was used, with the SQUID output coupled into a LC resonant tank, which served to match impedances and thereby improve sensitivity. A dc

bias current was sent to the SQUID, optimized in magnitude so as to maximize the $V(\Phi)$ transfer function. A small copper-wired loop placed around the device, or sometimes a thin-film superconducting loop fabricated on chip around the SQUID, was used to generate the ac modulation magnetic field, at a frequency of about 70 kHz. The ac SQUID output signal was phase sensitively detected with an analog lock-in amplifier referenced to the modulation field signal. The analog output of the lock-in amplifier was connected to a digital oscilloscope for data recording.

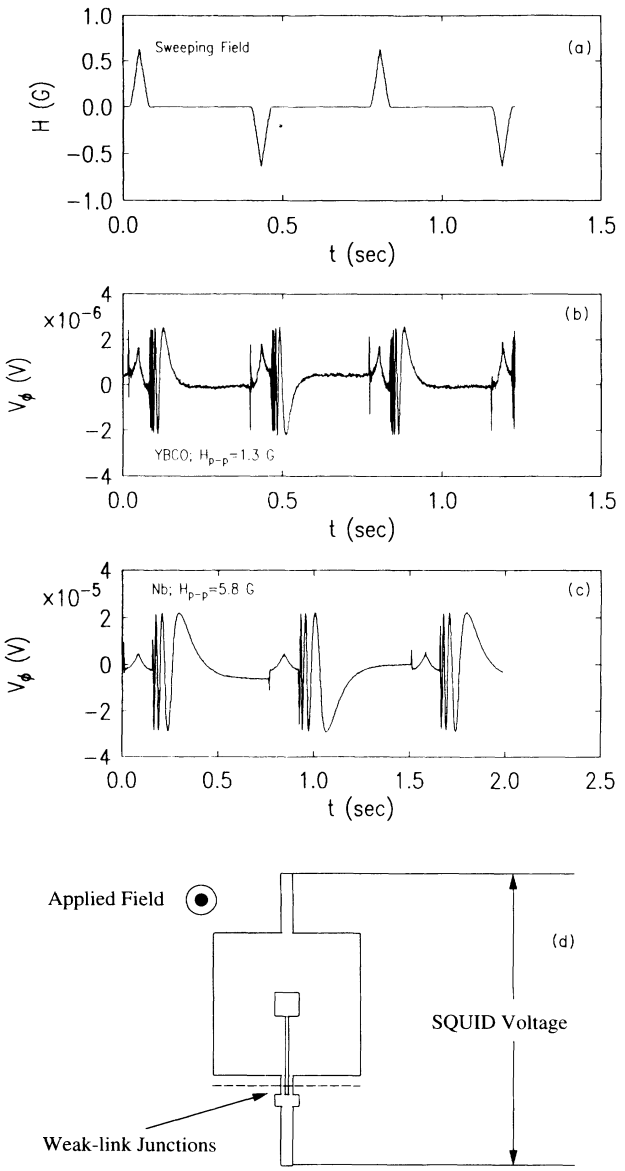

FIG. 3. Typical measurement signals. (a) Applied field's time dependence. (b) Typical output from a YBCO SQUID magnetometer in response to the applied field. (c) Output from a Nb SQUID magnetometer for comparison. The relaxation tail of the SQUID output is composed of two components. The first is from the decay of eddy current in adjacent copper structures on the test probe. After that is removed, a smaller tail with a different time constant persists. The tail part of the relaxation appears to be strongly temperature dependent, which makes us believe that it might be associated with the viscous motion of vortices that are trapped inside the washer. A sketch of the device geometry is presented in (d).

Samples under test were placed at the center of a copper-wire coil. The cycling magnetic field was generated by providing the magnet coil with a current wave form similar to that illustrated in Fig. 3(a). The hysteresis shift was determined from the shift of the SQUID output voltage during the zero field portion of the field sweep after the transient response (including the time-dependent hysteresis response) had decayed away. Examples of such output signals from a YBCO SQUID operating at 77 K and a Nb SQUID operating at 4.2 K are shown in Figs. 3(b) and 3(c), respectively. The general layout of the SQUID's used for these studies is given in Fig. 3(d). Special attention was paid to ensure the flatness of the "zero" floor of the cycling current input. This was done by placing a pair of back-to-back parallel-connected silicon diodes in series with the magnet coil, so that the threshold behavior of the diodes could isolate from the magnet coil the zero-voltage variation of the signal generator.

Measurements were conducted in a rf-shielded screened room, with the sample probe inserted in a μ-metal-shielded liquid-nitrogen or liquid-helium Dewar. The limiting sensitivity of the overall measurement environment was about $1-3\times10^{-7}$ G, with a 100-Hz bandwidth set on the lock-in amplifier, and upon an average of 10–50 traces on the digital oscilloscope. The stray magnetic signal from 60-Hz power lines was the limiting factor in the resolution of hysteresis.

RESULTS AND DISCUSSION

The hysteresis characteristic of a device is shown in Fig. 4 for a number of temperatures. The YBCO film of this device is 80 nm thick. In this device, the hysteresis δH appears to show multiple steps as a function of $H_{p\text{-}p}$. The steps for the 58-K data are indicated with arrows in the figure. We attribute the multiple steps to the possible existence of multiple sites around the washer structure at which the magnetic flux lines begin to penetrate, each site having a relatively well-defined local critical current density.

Assuming that each step represents the threshold field for a given site, and using Eq. (4), we can estimate the associated critical current density. In the inset the critical current density thus estimated is plotted as a function of temperature for the first two steps in the hysteresis data. This temperature dependence is consistent with what one obtains from direct measurement of the low-field critical current density for YBCO thin films in this temperature range. The magnitude of the critical current density indicates that, for this film, the weakest spot around the edge of the washer has a critical current at 77 K of around 5×10^5 A/cm^2, which is about an order of magnitude below what one would expect from direct transport measurements of the critical current density on such a film.

Below the first steps in Fig. 4, most notably for the 58-

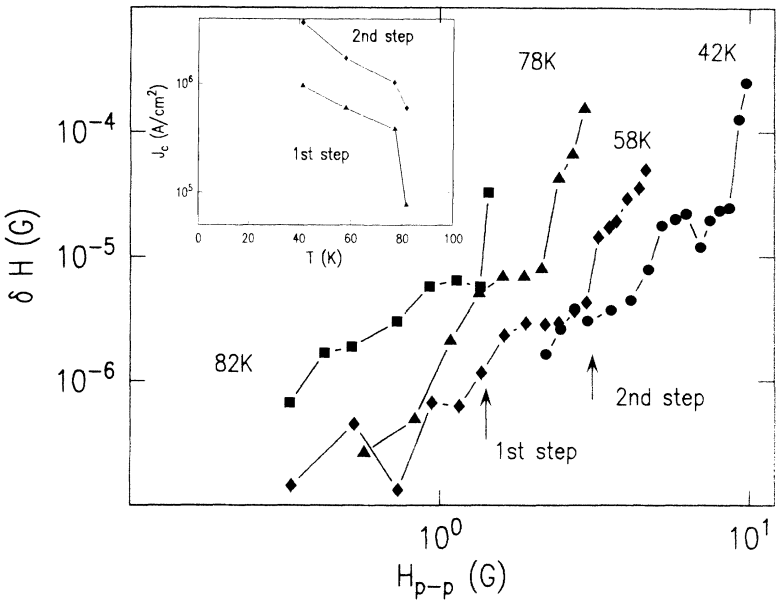

FIG. 4. Hysteresis shift δH of a YBCO SQUID as a function of peak-to-peak field $H_{p\text{-}p}$ for various temperatures. The film forming this SQUID is about 80 nm thick. At least two steps are present in these δH vs $H_{p\text{-}p}$ curves. The steps for the 58-K curve are indicated by the arrows. The inset shows the temperature dependence of the estimated critical current density associated with the two steps.

K data, there is some hysteresis at the level of $1-6\times10^{-7}$ G. We are not sure of the explanation for these low hysteresis tails seen in this curve and in some of our other data. These tails are near our measurement sensitivity limit. If they are real, there could be several possible explanations for them. They might be due to some averaging effect in the way we take data. They might be due to a locally degraded edge region. It might also be that some degraded edge regions can initially trap a vortex with an orientation that is not perpendicular to the film.

For most samples we measured, there was a point in applied field amplitude above which the hysteresis increased dramatically and became apparently random upon the cycling of the applied field (thus rendering trace averaging meaningless). A time-dependence trace of a device in such a state is shown in Fig. 5. We interpret this as the onset of flux entry at many sites around the washer, with all such sites having nearly the same pinning strength. Therefore, the value of the applied field at this point should, to a certain degree, correspond to the average critical current density of the material near the edge of the washer. This average critical current density should show less sample-to-sample variation, and should represent more closely the average film quality at the edge of the washer. Thus, it should be meaningful to compare the value of this threshold field for different samples.

We can, for example, use the threshold field associated with massive flux entry to study the dependence of hysteresis on the dimensions and film thicknesses of the washer structure. Shown in Fig. 6 are measurements at 77 K of hysteresis on three representative SQUID's with different thicknesses and different washer sizes. The upward arrow at the right end of each curve represents the threshold field above which massive flux entry occurs. The current density calculated using Eq. (4) with the

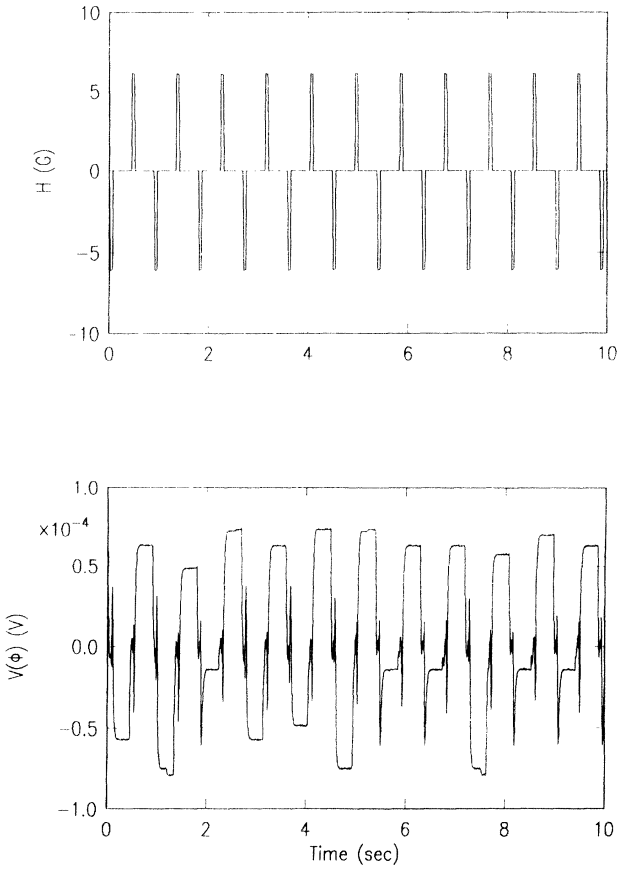

FIG. 5. An example of the time-dependent output of a SQUID magnetometer in response to the cycling applied field. The significant deviation from zero of the SQUID output during the zero-applied-field portion of the time is a sign of large hysteresis. The randomness of the SQUID output from cycle to cycle indicates different configurations of trapped flux.

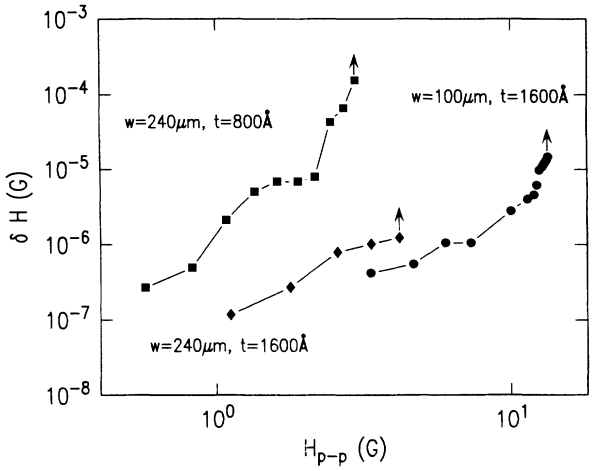

FIG. 6. Geometry dependence of the hysteresis. Larger washer sizes and thinner films in general result in larger hysteresis and lower threshold fields. The critical current density corresponding to the end point of these curves (where massive flux entry occurs) is about 10^6 Å/cm^2.

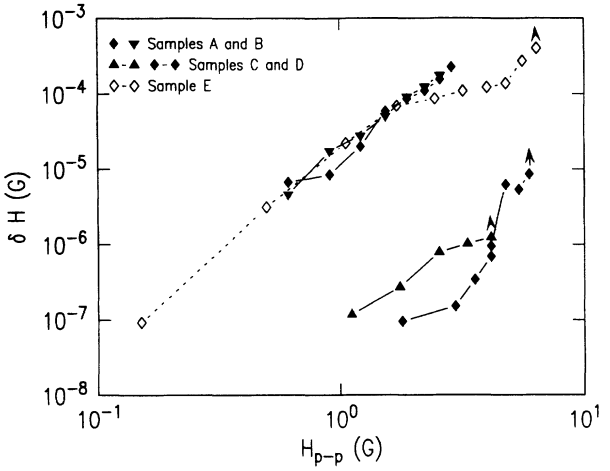

FIG. 7. Hysteresis of SQUID's prepared using the improved process compared to that of devices made with the old process. Samples *A* and *B*: 240-μm washer, 150-nm-thick films, were prepared before the improved process. Samples *C* and *D*: 240 μm, 160-nm films, were prepared with the improved process. SQUID *E* was made on the same chip as SQUID's *C* and *D*, but has a step-edge accidentally patterned cross a corner of the washer. This single step-edge weak-link caused its hysteresis to increase by more than two orders of magnitude.

thresholds for massive flux entry are, from left to right, 1×10^6, 1×10^6, and 3×10^6 A/cm^2 for the three samples. Trends that can be discerned are that a thicker film and a smaller washer result in less hysteresis and a higher threshold field. The exact scaling as predicted by Eq. (4), however, could not be established unambiguously from this set of data. Sample inhomogeneity and the possibility that a larger washer size may have a higher probability of encountering regions with weaker critical current may obscure the scaling behavior. The same argument can be used to explain why for most high-T_c SQUID's only hysteresis with a leading phase was observed. Because the outer rim of the washer structure is much longer in total length, it has a much greater chance of encountering defects. Thus it is much more likely that vortex penetration would first occur around the outer rim of the device, causing a hysteresis with a leading phase.

It is clear from the discussion above that inhomogeneity in microstructures and corresponding variations of local critical current density along the edge of the washer structure play a significant role in determining the overall hysteresis of the device. The presence of one local site with weak pinning can cause significant degradation of the overall hysteresis performance of the device. Such a weak pinning site, when located at only one edge of a structure, could cause a significant increase in hysteresis without showing much effect on a transport critical current measurement, if one could be made on the same line.

The dramatic effect of a single weak link on the hysteresis can be further illustrated by the data shown in Fig. 7. In Fig. 7, three sets of data are presented. The first set of data, *A* and *B*, is from measurements on samples prepared in earlier experiments before we improved our fabrication process. The second set, *C* and *D*, are from samples prepared using the improved fabrication process. An improvement of nearly three orders of magnitude in hysteresis in the field range of 1–5 G was obtained. Also shown in Fig. 7 is one special sample, *E*, prepared with the improved fabrication process, but having a step accidentally patterned into the edge of the washer structure due to a scratch on the photoresist mask during the preparation of the step-edge structure on the substrate (Fig. 8). The hysteresis characteristics of this device degraded by almost three orders of magnitude, simply due to the presence of this one single weak-link grain boundary cut into one corner of the washer structure.

In summary, we have demonstrated that the penetration of magnetic flux at the edges of the pickup washer structure causes magnetic hysteresis in SQUID magnetometers. There are three important interactions that determine the onset of such hysteresis—the Lorenz force from the induced shielding current circulating around the edge, the interaction between an edge-boundary-condition-related image vortex and a real vortex, and the pinning force on the vortex resulting from its interaction with a defect. The balance of these three forces results in a threshold field H_{Ta}. In the thin-film limit where a 2D description of a vortex is applicable, the threshold field should scale as $(J_c d)^{3/4}/\sqrt{R_2}$, where $J_c d$ is the sheet critical current of the film at the edge where flux penetration first occurs. The sheet critical current is a convenient way of measuring the strength of defect-vortex-interaction-related pinning. Process improvements undertaken during the course of these experiments with the intention of improving edge film quality resulted in a three-orders-of-magnitude reduction of hysteresis δH compared to our earlier results.

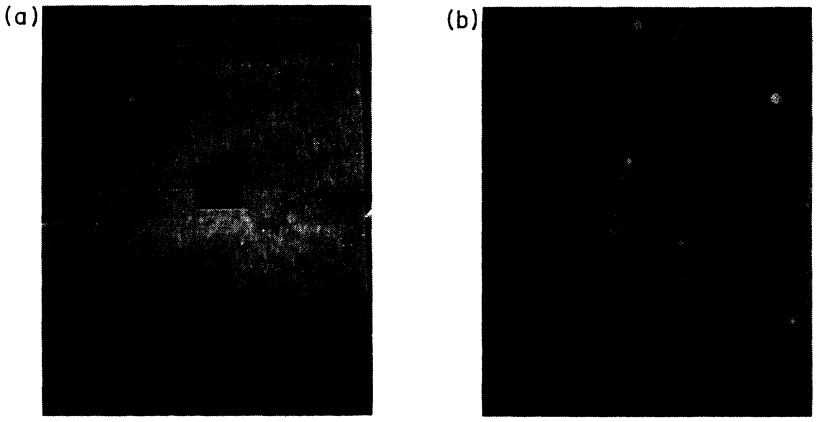

FIG. 8. (a) A scanning-electron micrograph of SQUID E in Fig. 7. (b) At higher magnification, it shows the presence of a step-edge weak-link at one corner of the washer.

From the data presented in Fig. 7, we conclude that the hysteresis of the device is determined by the weakest spot around the edge of the washer structure of the device. One single weak-link boundary, cutting across the edge of the device, is enough to cause a significant increase in hysteresis. A film with high average critical current is necessary but not sufficient for the making of low hysteresis SQUID's. The edge quality of the finished device is important. This concept also holds true for other device structures where flux entry and/or flux-entry-related dissipation are of concern. One special example worth noting is that of the high-rf power performance of thin-film microwave resonators. It is quite possible, in our opinion, that the additional loss incurred in such devices at high-power levels is due to the entry of magnetic vortices around the edges of a resonating strip-line structure. The flux-entry process in that case is very similar to what we studied here. Therefore, for such devices, it is important to recognize the importance of low-edge defect densities and to correlate the device performance to the local properties of the film at the edge of the device. Some of our preliminary studies on thin-film strip-line resonator structures fabricated using a process similar to that for our low hysteresis SQUID's show that such resonators do appear to have better high-power properties compared to devices made of films of same thickness but fabricated using other methods.[23]

ACKNOWLEDGMENTS

The authors wish to thank K. Stawiasz, R. L. Sandstrom, C. Jessen, J. Rozen, M. B. Ketchen, and D. E. Oates for assistance during various stages of the experiment, as well as for useful discussions. This work is supported in part by the Office of Naval Research under Contract No. N00014-92-C-0193, and was conducted under the auspices of and with partial support from the Consortium for Superconducting Electronics, which is partially supported by the Advanced Research Projects Agency (Contract No. MDA972-90-C-0021).

APPENDIX

In this Appendix we give expressions for the threshold field of a thin-film circular loop and the threshold current for a thin-film wire carrying a current in its self-field. For a circular-shaped input area with radius R, bounded by a single turn coil of a thin-film strip with thickness d ($d<\lambda$, where λ is the London penetration depth) and width w, with $w \ll R$, when a uniform field is applied, the spatial distribution of the current flow in the superconducting strip can be approximated, to the lowest order, by Eq. (3.08-1) in Ref. 24. An edge current density can thus be estimated. Using Eq. (3), the threshold field corresponding to the penetration of a vortex into the superconducting strip becomes

$$H_{\mathrm{Ta}}=0.499\sqrt{w/R}\,[\ln(16R/w)-1.75]\left[\frac{\Phi_0}{R^2}H^{*3}\right]^{1/4}. \tag{A1}$$

In a more general case, the threshold current a thin-film superconducting strip can carry in a weak magnetic field can also be estimated the same way. Again using Eq. (3.08-1) in Ref. 24 for a stripline carrying the total current I, we have sheet current density for a point at a distance δ away from the edge of the strip,

$$K_L(\delta)=\frac{I}{\pi w}\sqrt{w/\delta}\,, \tag{A2}$$

where we assumed $\delta \ll w$. Equation (A2) combined with the pancake vortex's image force near the edge as calculated using the interaction derived in Ref. 9,

$$K_I(\delta)=\frac{\Phi_0 c}{16\pi^2\delta^2}\,, \tag{A3}$$

gives the equation for the threshold in current I_T as the value of I when the maximum magnitude of combined driving force as defined by

$$K_e(\delta)=\frac{\Phi_0 c}{16\pi^2\delta^2}-\frac{I}{\pi w}\sqrt{w/\delta} \tag{A4}$$

first exceeds the sheet critical current at the edge of the strip. This gives

$$I_T=(J_c dw)\left[1.55512\left[\frac{\Phi_0 c}{w^2 dJ_c}\right]^{1/4}\right]$$
$$=(J_c dw)\left[2.4621\left[\frac{\Phi_0/w^2}{H^*}\right]^{1/4}\right]. \quad \text{(A5)}$$

The current I_T determines the point, where massive flux entry could occur. This is relevant for estimating the onset of hysteresis loss in superconducting thin-film stripline structures for applications such as high-power microwave resonators.

[1]R. H. Koch, M. B. Ketchen, W. J. Gallagher, R. L. Sandstrom, and A. W. Kleinsasser, D. R. Gambrel, T. H. Field, and H. Matz, Appl. Phys. Lett. **58**, 1786 (1991).

[2]J. W. Purpura, T. R. Clem, and R. F. Wiegert, IEEE Trans. Appl. Supercond. **3**, 2445 (1993).

[3]T. R. Clem, J. W. Purpura, and R. F. Wiegert, IEEE Trans. Appl. Supercond. **3**, 1848 (1993).

[4]J. Z. Sun, W. J. Gallagher, and R. H. Koch, Appl. Phys. Lett. **61**, 3190 (1992).

[5]J. Z. Sun, W. J. Gallagher, and R. H. Koch, IEEE Trans. Appl. Supercond. **3**, 2022 (1993).

[6]J. Z. Sun, W. J. Gallagher, and R. H. Koch (unpublished).

[7]J. Z. Sun, W. J. Gallagher, and R. H. Koch (unpublished).

[8]V. Foglietti, R. H. Koch, W. J. Gallagher, B. Oh, B. Bumble, and W. Y. Lee, Appl. Phys. Lett. **54**, 2259 (1989).

[9]E. H. Brandt and M. Indenbom, Phys. Rev. B **48**, 12 893 (1993).

[10]E. Zeldov, J. R. Clem, M. McElfresh, and M. Darwin, Phys. Rev. B **49**, 9802 (1994).

[11]J. Zhu, J. Mester, J. Lockhart, and J. Turneaure, Physica C **212**, 216 (1993). This work describes an exact solution of the field and current pattern in disk-shaped superconductors under certain assumptions and neglecting the discreteness of vortices.

[12]M. W. McElfresh, Y. Yeshurun, A. P. Malozemoff, and F. Holtzberg, Physica A **168**, 308 (1990).

[13]V. N. Kopylov, A. E. Koshelev, I. F. Schegolev, and T. G. Togonidze, Physica C **170**, 291 (1990).

[14]M. Konczykowski, L. I. Burlachkov, and Y. Yeshurun, Phys. Rev. B **43**, 13 707 (1991).

[15]L. Burlachkov, Phys. Rev. B **47**, 8056 (1993).

[16]L. Burlachkov, Y. Yeshurun, M. Konczykowski, and F. Holtzberg, Phys. Rev. B **45**, 8193 (1992).

[17]Mark B. Ketchen, W. J. Gallagher, A. W. Kleinsasser, S. Murphy, and John R. Clem, *SQUID'85—Superconducting Quantum Interference Devices and Their Applications,* edited by Hahlbohm and H. Lubbig (Gruyter, Berlin, 1985), p. 865.

[18]John R. Clem, Phys. Rev. B **43**, 7837 (1991), and references therein.

[19]J. R. Clem, in *Low Temperature Physics-LT13,* edited by K. D. Timmerhaus, W. J. O'Sullivan, and E. F. Hammel (Plenum, New York, 1974), Vol. 3, p. 102.

[20]C. P. Bean and J. D. Livingston, Phys. Rev. Lett. **12**, 14 (1964).

[21]J. R. Clem, J. Appl. Phys. **50**, 3518 (1979).

[22]J. Z. Sun, W. J. Gallagher, A. C. Callegari, V. Foglietti, and R. H. Koch, Appl. Phys. Lett. **63**, 1561 (1993).

[23]D. E. Oates (private communication).

[24]T. Van Duzer and C. W. Turner, *Principles of Superconductive Devices and Circuits* (Elsevier, North-Holland, Amsterdam, 1981), p. 107.

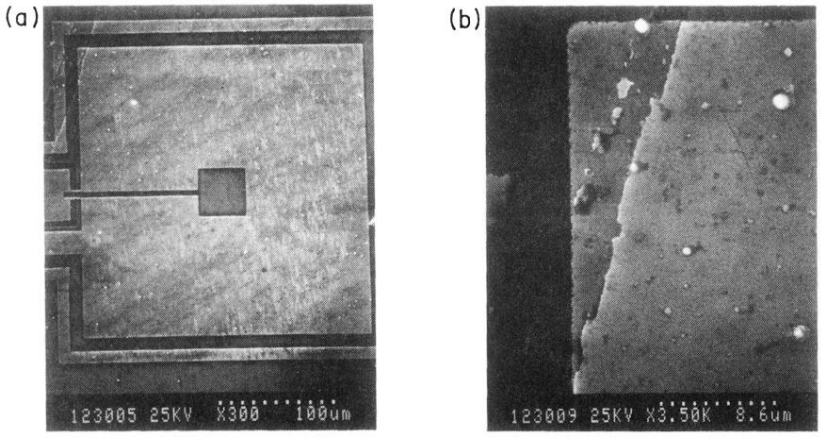

FIG. 8. (a) A scanning-electron micrograph of SQUID *E* in Fig. 7. (b) At higher magnification, it shows the presence of a step-edge weak-link at one corner of the washer.